JOURNAL OF MATERIALS SCIENCE 21 (1986) 365–379

Review
The chemical and electrochemical stability of beta-alumina

R. O. ANSELL
Department of Chemistry and Metallurgy, Glasgow College of Technology, Cowcaddens Road, Glasgow G4 0BA, UK

The factors which influence the stability of sodium ion conducting beta-alumina ceramics are reviewed from the standpoint of their major application, the sodium–sulphur battery. Significant progress towards understanding the degradation of the ceramic has been made in recent years.

1. Introduction

Materials from the beta-alumina family ($Na_2O \cdot xAl_2O_3$ where x lies between 5 and 11) have been widely investigated for application as ionic conductors in the sodium–sulphur high temperature (300 to 350° C) secondary battery. A recent review by Stevens and Binner [1] gave a detailed account of the structure and properties of beta-aluminas from a fabrication view point. The major barrier to the successful exploitation of the beta-aluminas in sodium–sulphur cells has been the reliability of the cell and principally the beta-alumina ceramic in the cell. This review deals with the work which has been carried out on the stability of the beta-alumina in the sodium–sulphur cell. It concentrates on the modes of degradation to be expected in commercially produced materials in sodium–sulphur cells. To this extent it is mainly concerned with polycrystalline beta-alumina which may be regarded as a mixture of beta-($Na_2O \cdot 11Al_2O_3$) and beta″-($Na_2O \cdot 5Al_2O_3$) often with a very high ratio of beta″/beta (beta″ > 90%) and the interaction of this material with cell materials and operating conditions.

The principal modes of degradation are: (a) those arising from the electrochemical and chemical effects of sodium; (b) those arising from possible reactions with sulphur and sodium polysulphides; (c) those arising from the influence of the applied potential on beta-alumina (in particular anodic degradation); and (d) those associated with the influence of impurities (for example foreign ions and water).

The effects of degradation which are observed in practice are: (a) ceramic cracking; (b) non-faradic cells; and (c) cell resistance rise.

From the point of view of the user of sodium–sulphur batteries there are three major concerns: (a) that the cell resistance should be low and stable; (b) that the cell should not fail prematurely; and (c) that the cell capacity should be maintained.

It can be seen that many of the effects that are detrimental for the battery user can arise from degradation of the ceramic. Possibly the most important of these is that the cell failure should not occur prematurely and it is the relation between cell failure and the mode of ceramic degradation which has been most widely studied. The separate types of degradation will be discussed individually in the following sections.

2. Sodium electrode modes of degradation

2.1. Chemical effects

2.1.1. Stress corrosion cracking in liquid sodium

Early studies [2] indicated that the beta″-alumina compositions were stable to attack by sodium but that cells failed under electrolytic conditions [2, 3]. Investigations of stress corrosion cracking of beta-alumina shows the absence [4, 5] of stress assisted dissolution of beta-alumina in sodium. Shetty *et al.* [4] investigated two compositions of beta″-alumina, one containing 8.8%* Na_2O–0.75% Li_2O balance Al_2O_3 and the other containing 10% Na_2O–1.2% Li_2O balance Al_2O_3. The latter composition was chosen because it had a low critical current density for failure in electrolytic tests.

A double cantilever beam specimen geometry was used to study subcritical crack growth. The tests were carried out in sodium at 300° C after holding at 375° C to allow sodium wetting of the specimens. The subcritical crack growth data for the two compositions gave linear plots of log V against K_I which fitted the equation

$$V = AK_I^n \quad (1)$$

where V is the crack velocity, A is an empirical constant, K_I is the stress intensity factor and n is an empirical exponent.

The large value of n observed (n = 562 and 355) discounts any serious stress corrosion cracking (SCC) in the lower soda composition. The higher soda composition showed an increased susceptibility to stress corrosion cracking with n = 34 and 119.

Davidge *et al.* [5] found that polycrystalline beta-alumina of composition 8% Na_2O–2.0% MgO

*All compositions given in wt%.

0022–2461/86 $03.00 + .12

balance Al_2O_3 which had approximately equal proportions of β or β'' alumina showed remarkably low time dependence of strength under stress. They employed both constant strain rate tests in air and in liquid sodium at 300° C. They also carried out constant stress tests in liquid sodium at 300° C in order to investigate delayed fracture. A consistent strain rate sensitivity of strength was not found and this was taken to indicate a very high value of n in Equation 1.

The delayed fracture tests, which were expected to give results of more significance because of the longer time scale of testing, showed (unexpectedly) that the mean strength in delayed fracture was 203 MNm^{-2} as opposed to 196 MNm^{-2} for the strain rate measurements. This showed that stress corrosion cracking was not occurring under these conditions. Although there was little time dependence of strength it was found from the strain rate tests in air and liquid sodium that the strength of the ceramic was significantly lower in liquid sodium (265 $\pm$ 53 MNm^{-2}, 51 samples in air 196 $\pm$ 43 MNm^{-2}, 47 samples in liquid sodium). The results were obtained on samples randomly selected from a number of tubes from different powder batches.

When 40 samples from a single tube were tested in air at 20° C and two different strain rates the Weibull modulus obtained was ~ 8 and the mean strength at the high strain rate was 312 MNm^{-2} and at the low strain rate 297 MNm^{-2}. This allows the determination of n as 150 in Equation 1.

The beta-alumina consequently had a very low time dependence of strength under stress compared with other oxide ceramics. The results were consistent with those of Shetty *et al.* [4]. The conclusions were that stress corrosion cracking does not occur in liquid sodium, that current focusing under electrolytic conditions has a significant role in electrolytic degradation, that short term tests could be used with confidence in design of beta-alumina electrolytes and that proof testing could be used to eliminate weak tubes without significantly weakening the surviving tubes.

2.1.2. Sodium wetting of beta-aluminas

Despite the lack of evidence of stress corrosion cracking there is evidence of chemical affinity between sodium and beta-alumina. This is shown by the ease with which beta-alumina is wetted at elevated temperatures. Gibson [6] and Viswanathan and Virkar [7] have investigated the wetting of beta-alumina in sodium. One possible effect of wetting on beta-alumina fracture was to reduce the thermodynamic surface energy for ideal fracture and Davidge *et al.* [5] point out that this could explain the reduction in strength of the beta-alumina samples immersed in sodium. The importance of adequate wetting of beta-alumina for good cell performance was recognized early on and first studied in detail by Gibson [6]. He employed a radiographic technique to examine the contact angles of the beta-alumina tubes which had been immersed in sodium in sealed containers at the appropriate temperature and subsequently quenched.

Viswanathan and Virkar's [7] method was the direct observation of the contact angle of a sessile drop. They found that the contact angle was very sensitive to prior exposure of the ceramic to moisture. For lithia stabilized beta-alumina 8.8% Na_2O–0.75% Li_2O, balance Al_2O_3 the results of Viswanathan and Virkar are given in Table I. The beta-alumina did not dewet on reduction of the temperature. The area of the beta″-alumina disc beneath the sodium was darkened and the extent of darkening was lower for drops that did not wet well. Scanning electron microscopy (SEM) showed that the darkened area was smoother than the rest of the disc which implied beta-alumina dissolution in sodium. Sodium–sodium cells were used to investigate the effect of moisture and poor wetting. (These cells allow electrolysis of sodium ions through beta-alumina between sodium electrodes and simulate the conditions in sodium–sulphur cells without the complication of the sulphur electrode.) Cells that were baked at 450° C in vacuum prior to sodium filling passed 1000 A h cm^{-2} at 4 A cm^{-2} and 400° C. The cells that were not baked failed after 200 A h cm^{-2} in similar conditions. The presence of moisture and hence lack of wetting reduced cell life.

TABLE I The contact angle of sodium on beta″-alumina*

Treatment	Sample temperature (° C)	Contact angle (deg)
Unbaked	260	160
	360	90
	425	25
Baked at 425° C	200	50
in vacuum for	360	0
60 h	400	0
Kept at 100% r.h.	360	103
at 25° C for 24 h	420	90

* After Viswanathan and Virkar [7].

2.1.3. Chemical colouration of beta-aluminas in sodium

The darkening of beta-aluminas in sodium was the subject of earlier studies by Demott and Redfern [8]. They measured the thermoluminescence of samples blackened by sodium immersion and by electrolysis in sodium–sodium cells. Some samples were irradiated with X-rays. The glow curves of ceramic which had not been irradiated did not show thermoluminescence below the temperature of the onset of black body radiation. Both the electrolysed and untreated ceramics showed two thermoluminescence peaks after irradiation. The light emitted in each peak was of the same wavelength 505 nm and this indicated that two electron traps (0.8 and 1.1 eV) which could form F centres were present. The predominance of one or other trap depended on ceramic composition. There was a reduction in the population of the deeper trap (1.1 eV) in the darkened ceramic. No evidence of colour centres was found in material which had not been subjected to irradiation.

Demott and Redfern found that it was possible to bleach the blackened beta-alumina by heating in air. The ceramic blackened by immersion in sodium required heating to a higher temperature than the electrolysed ceramic. This was believed to indicate

that the two types of blackening were different. More recent examination [9] of the ceramic extracted from sodium–sodium cells shows that if care was taken over sample preparation the extracted ceramic was violet in colour showing the presence of colour centres. De Jonghe and Buechele in a detailed study [10] of the chemical colouration of beta-alumina attribute the colouration to the reduction of beta-alumina by sodium. The reduction introduces oxygen vacancies which are compensated by electrons and the colouration extends as a layer from the sodium/electrolyte interface. The reaction is given as [11]

$$2Na_E + (O_0)_\beta \rightarrow (Na_2O)_E + (V_0^{\cdot\cdot})_\beta + 2(e')_\beta \quad (2)$$

where Kroger–Vink notation is used, the subscript β refers to beta-alumina and the subscript E to the sodium electrode in which the oxygen dissolves. Experiments [10] were carried out on single crystals of beta-alumina and polycrystalline beta-alumina. Silver exchange [12] was used to enhance the colouration profiles of the polycrystalline samples. The rate of propagation of the colouration front was measured from the normalized microdensitometer trace of the micrograph of the coloured sample. The value of x the distance at which the darkening was half the maximum value was determined as a function of immersion time of the beta-alumina in sodium. This distance x was linearly dependent on the square root of the immersion time and the rate was substantially faster for the 10 μm grain size as opposed to the 150 μm grain size ceramic. The colouration producing defects were transported rapidly within the grain boundaries. For beta″-alumina the lattice diffusion coefficient was at 350° C,

$$D_{\text{lattice}} \leqslant 10^{-10}\,\text{cm}^2\,\text{sec}^{-1}$$

and

$$D_{\text{boundary}} = 9.8 \times 10^{-7}\,\text{cm}^2\,\text{sec}^{-1}$$

In single crystals of beta-alumina the colouration occurred as a discrete layer and propagation rates were measured directly. The thickness of the coloured layer x_s was linearly dependent on the square root of the sodium immersion time. The value of the constant K, where $K = x_s^2/2t$ and t is the time of immersion, was $K = 1.1 \times 10^{-10}\,\text{cm}^2\,\text{sec}^{-1}$ at 300° C and $K = 3.4 \times 10^{-10}\,\text{cm}^2\,\text{sec}^{-1}$ at 350° C. The activation energy for defect propagation was about 67 kJ mol^{-1}. For beta-alumina single crystals the effective colouration defect propagation rate was $4.5 \times 10^{-10}\,\text{cm}^2\,\text{sec}^{-1}$.

Transmission electron microscopy (TEM) of the coloured beta″-alumina did not show any features that could be attributed to colouration and it was decided that the process involved point defects rather than second phases. Experiments with single crystals showed that colouration proceeded isotropically. The removal of colouration by heating in air at 300° C, "bleaching", occurred in a well defined layer and only in the direction of the conduction planes. In the absence of air the heating did not produce bleaching. It was concluded that the colouration involved removal of oxygen from the beta-aluminas whilst bleaching in air involved a reoxidation. Colouration also involved electrons since it produced a broad optical absorption and other workers (Weber [13]) had measured increased electronic conductivity in the blackened material. The isotropic colouration and non-isotropic bleaching was thought to arise from differences in the oxygen vacancy ($V_0^{\cdot\cdot}$) diffusion rate in the spinel blocks and the conduction planes. This was believed to depend on the oxygen partial pressure. At high oxygen partial pressures $V_0^{\cdot\cdot}$ diffusion in the spinel blocks is low because of the small number of $V_0^{\cdot\cdot}$ present. At low oxygen partial pressures (reducing conditions) $V_0^{\cdot\cdot}$ diffusion through the spinel blocks would be expected. Structural considerations would mean that the conduction plane $V_0^{\cdot\cdot}$ mobility would not be so affected. The injection of $V_0^{\cdot\cdot}$ into the spinel blocks was shown by masking the single crystal with glass, so that reduction could not occur along the conduction planes, and immersing the sample in sodium. The darkening produced indicated that colouration could occur through the spinel blocks.

Attempts at photodarkening the beta-alumina by irradiation with ultraviolet light did not produce darkening, showing that darkening was not simply the effect of a sodium ion and electron pair. On the basis of the activation energy for the process, which was half that for electron transport, it was concluded that $V_0^{\cdot\cdot}$ transport was the rate controlling factor in colouration. No effect of water absorption on the bleaching or colouration was observed. Perhaps the most important finding was that it was possible for the colouration of the beta-alumina to introduce a variation in the electronic conductivity of beta-alumina. This could lead to a variation in the electronic/ionic transport number ratio which can under certain conditions lead to the formation of sodium within the ceramic and its consequent failure. This mode of failure is discussed in detail in section 2.2.1.

2.1.4. Electron spin resonance (ESR) identification of defects in blackened beta-aluminas

Gourier *et al.* [14], carried out an ESR study of beta-alumina and beta″-alumina which had been exposed to sodium and also ceramic which had been electrolysed in sodium–sodium cells. They found that prior exposure of the ceramic to sodium had a dramatic effect on sodium–sodium cell durability with cell life falling from 350 A h cm^{-2} for no prior exposure to 0 A h cm^{-2} for 4 weeks prior exposure to sodium at 330° C. They found that the ESR spectrum of blackened material had a weak line superimposed on the Mn(II) spectrum. (The Mn(II) line arises from low levels of impurity ~ 10 p.p.m.). This line was attributed to the conduction electrons of metallic sodium. The signal line width suggested that the sodium particle size was less than 0.5 μm. The fact that the signal was not removed after 3 h immersion of the sample in water indicated that the sodium was present in the bulk.

Barrett *et. al.* [15], extended the study of the sodium defects to several different types of interaction with sodium; additive colouration in sodium or

potassium vapour, simple immersion in liquid sodium and electrolytic colouration at the cathode (either with a blocking counter electrode or a sodium nitrate solution). In addition they investigated ceramics from failed sodium–sodium and sodium–sulphur cells which had been cycled at 80–100 mA cm^{-2} for 100 to 600 charge/discharge cycles. Three types of defect were observed, a single electron trapped at an unknown lattice site, ultra-small sodium particles and large sodium particles of about 1 μm size. In polycrystalline beta-ceramics and beta″-ceramics the trapped electron and ultra-small sodium particles were found after exposure to sodium or potassium vapour or sodium liquid. Ultra-small sodium particles and large sodium particles were present in the electrolytic tests. All three defects were present in sodium–sodium tested ceramic. Only the trapped electron was found in ceramic from sodium–sulphur cells, although the more aggressive extraction required to obtain the ceramic free of polysulphides could have influenced this. Sodium beta-alumina single crystals gave only ultra-small sodium particles or defects when used in the sodium liquid, sodium vapour, potassium vapour and blocking electrode tests.

The stability of the defects was determined by thermal treatment in air at increasing temperatures followed by ESR observation. The ESR signal due to large sodium particles disappeared during the first thermal step at 100° C. The thermal bleaching of the small sodium particle signal occurred at 600° C and that of the trapped electron at 700° C. The colour of the sample was still violet when the ultra-small sodium signal disappeared at 600° C so the colouration was associated with the single trapped electron. Further experiments on vacuum thermal treatment of the previously tested ceramics suggested that the bleaching of the beta-alumina in air occurred not by removal of the trapped electron but by conversion of the trapped electrons into ultra-small sodium particles, by combination with sodium ions, followed by the bleaching of these.

The most likely explanation [15] of the effect of alkali metal vapour on the beta-alumina was the formation of electron compensated oxygen vacancies which was also envisaged by De Jonghe and Buechele [10]. The point defect was probably a diamagnetic F centre (an oxygen vacancy compensated by two electrons). These F centres probably combined with sodium ions in the conduction planes to form the ultra-small sodium particles. The ESR signal was throught to arise from the trapping of the electrons compensating the oxygen vacancy.

The formation of ultra-small sodium particles by chemical and electrochemical colouration was similarly interpreted. The injected electrons were trapped at oxygen vacancies which drifted toward the negative electrode. This was supported by the evolution of gas (believed to be oxygen) at the positive electrode which implied that the oxygen ions moved to the positive electrode. The electrons associated with oxygen vacancies then combined with sodium ions to form colloidal sodium particles. The large sodium particles observed in electrolytic tests were probably a result of aggregation of the small particles under the influence of local cathode conditions.

2.1.5. Oxygen interstitial transport in beta-alumina

The role of oxygen interstitial transport was investigated by De Jonghe *et al.* [16]. They found that the single crystals of beta-alumina chemically coloured by sodium at 350° C had a maximum in the graph of the logarithm of the parabolic bleaching rate constant K against temperature at 250° C. They established, by consideration of the flux of oxygen ions into the beta-alumina and the flux of electrons out of beta-alumina during bleaching, that ion diffusion would control the rate and gave an upper bound for the oxygen ion diffusion coefficient $D_{ion} = 5 \times 10^{-14} cm^2 sec^{-1}$. The anomaly in the bleaching rate was then explained in terms of an irreversible conversion of the oxygen interstitials into trapped interstitials between 300 and 350° C.

The oxygen diffusivity in beta-alumina and beta″-alumina was determined by McHale *et al.* [17], who used isotopic oxygen exchange. The diffusion profiles which resulted were measured using secondary ion mass spectrometry (SIMS). Their studies were carried out under equilibrium conditions betwen 300 and 350° C. The diffusion profiles obtained corresponded to very slow surface exchange kinetics followed by relatively rapid oxygen diffusivity. The diffusion equation was solved by making the assumption that the rate of exchange of oxygen at the surface was proportional to the difference between the concentration in the gas and the concentration in the surface at any given time. Using this boundary condition in the equation for a semi-infinite medium allowed the calculation of the diffusion coefficients. For beta-alumina there was a second component in the diffusion profile, probably due to surface microcracks, which gave rise to an error for the sample at 425° C. The best linear fit to the data for the variation of diffusion coefficient (D) with temperature, T gave

$$D = 1.2 \times 10^{-5} \exp\left[-\left(\frac{1.1(eV)}{kT}\right)\right] cm^2 sec^{-1},$$

for beta-alumina

and

$$D = 2.2 \times 10^{-6} \exp\left[-\left(\frac{2.6(eV)}{kT}\right)\right] cm^2 sec^{-1},$$

for beta″-alumina

The value for beta-alumina is in agreement with the upper limit for interstitial oxygen diffusion found by De Jonghe *et al.* [16].

The activation energy for oxygen diffusion in beta″-alumina is too high for an extrinsic interstitial mechanism. McHale *et al.* [17], suggested that, since the conduction plane in beta″-alumina is relatively close packed, the mechanism was not interstitial but included a defect formation enthalpy characteristic of a vacancy diffusion mechanism.

2.2. Electrolytic degradation

Two main types of electrolytic degradation have been

identified. The first Mode I degradation [2–4] occurs through the focusing of sodium ions in the solid electrolyte to the sodium filled tips of pre-existing surface flaws. The Poiseuille pressure resulting from the flow of sodium out of the flaw causes cracking of the ceramic. The second, Mode II degradation [11, 18, 19] occurs as a result of the development of electronic conductivity in the beta-alumina as a result of the reaction with sodium. This leads to a gradient in the ionic/electronic transport number ratio in the beta-alumina and the possibility of the formation of sodium metal within the ceramic during cell charging. This results in internal pressure and microcracking of the ceramic. The Mode II degradation is discussed first because of its close relationship to the chemical reaction of sodium with beta-aluminas.

2.2.1. Internal sodium deposition – Mode II degradation

This mode of degradation takes place during the charging of the cell at the sodium electrode–beta-alumina interface. It is believed [18] that electron injection into the solid electrolyte from the sodium electrode during charging causes the internal deposition of sodium in the electrolyte. The experimental observation of Mode II degradation [18] was made on ceramics which had a composition of 9.6% Na_2O–0.25% Li_2O, balance Al_2O_3 which had been manufactured and tested at the General Electric Research and Development Centre. They had been subjected to a current density of 100 mA cm^{-2} during cycling in sodium–sulphur cells at 300° C. Ceramics were examined by optical microscopy using a silver staining technique [12] after a total charge passage of 23 to 703 A h cm^{-2}. Progressive but uneven ceramic darkening was observed and there were no significant features apart from the variation in the extent of darkening on the silver stained sodium electrode surface of the ceramic. Observation of the section of the ceramic showed that electrolyte damage had occurred in an even layer like manner from the sodium electrode interface. The damage consisted of regions of microfracture and these were found (by analysis with SEM, analytical transmission electron microscopy (ATEM) and high voltage transmission electron microscopy (HVTEM) to be associated with internal sodium deposition. The Mode II degradation was slow (after 703 h of charge passage the damaged region was approximately 0.5 mm thick) as compared to Mode I failure which was rapid once the critical conditions were achieved.

De Jonghe *et al.* [18] recognized that electron injection was unlikely at the fields which would be attained in cell operation (10 V cm^{-1}) since the field required for electron injection must exceed the band gap (9.0 eV for beta-alumina). The chemical colouration process discussed earlier (Section 2.1.3) would, however, lead to significantly increased electronic conductivity. The additional requirements for internal deposition were: (a) a driving force for ceramic microfracture; and (b) an ionic/electronic transport number gradient.

The first requirement would be fulfilled by the applied charging voltage and the latter would arise if the electrolyte were not in equilibrium with the electrodes. Such lack of equilibration is clearly demonstrated by the uneven extent of colouration. The Mode II mechanism would be expected to involve the polarization and condition of the sulphur electrode during cell operation. It would be less likely to be observed in the sodium–sodium cell where transport number gradients should be minimal. The detailed theoretical analysis of the Mode II degradation is given in papers by De Jonghe [11, 19].

2.2.2. The focusing of current to pre-existing surface flaws – Mode I degradation

This type of degradation occurs at the sodium electrode beta-alumina interface when the cell is charged. The pre-existing surface flaws filled with liquid sodium form a low resistance path for the sodium ions to be discharged. The discharge of the ions at the tips of the surface cracks leads to a flow of sodium out of the crack. The flow of sodium causes a Poiseuille pressure at the crack tip which results in the failure of the ceramic. Considerable attention has been given to this mode of failure since its discovery [2, 3]. The detailed models of Mode I failure will be discussed individually.

2.2.3. The Armstrong–Dickinson–Turner (A–D–T) model

Armstrong *et al.* [3] proposed a model in which the current was focused towards the sodium filled flaws (Fig. 1) in the same way as dendrites are formed at the cathode during metal deposition in an aqueous solution. The dendrite growth within the ceramic was therefore controlled by the electrolyte resistance. The path for dendrite growth in the ceramic was created by fracture as a result of stress near the tip of the pre-existing surface crack. The driving force for cracking of the ceramic was the Poiseuille pressure arising from sodium flow out of the microcrack under electrolysis.

$$\Delta P = \frac{8\eta i V_m l^2}{nF r^3} \quad (3)$$

where ΔP is the Poiseuille pressure, η is the coefficient of viscosity of sodium, i is current density, V_m is molar volume, l is the crack length, r is the radius of crack tip, n is the number of electrons and F is Faraday's constant.

Fracture occurred if the pressure exceeded the critical stress σ_c given by the Griffith criterion.

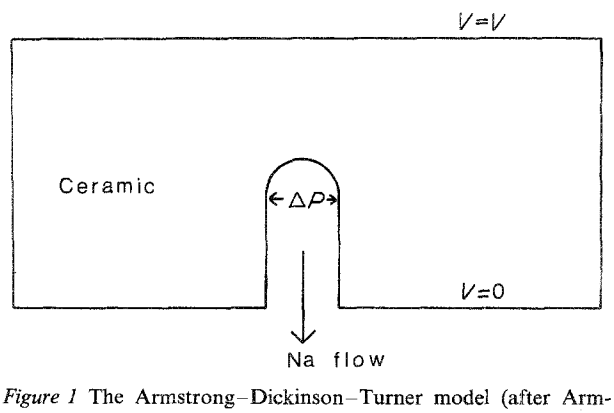

Figure 1 The Armstrong–Dickinson–Turner model (after Armstong *et al.* [3]).

$$\sigma_c = \left[\frac{2E\gamma}{\pi(1 - \nu^2)l}\right]^{1/2} \quad (4)$$

where E is Young's modulus, γ is the surface energy and ν is Poisson's ratio.

The Poiseuille pressure dropped after crack extension and the crack subsequently filled and extended again. One of the features of the model was that the crack would only extend if the dimensions exceeded the critical value for fracture. For a 10^{-7} cm crack diameter and a current of $100\,\text{mA cm}^{-2}$, $\Delta P = 150\,\text{MNm}^{-2}$ when the crack length was equal to 5×10^{-4} cm. The model is essentially a critical fracture model in which catastrophic failure does not occur because of the reduction of the Poiseuille pressure on crack extension.

2.2.4. The Richman–Tennenhouse (R–T) model

Richman and Tennenhouse argue [2] that solution and diffusion of the ceramic in liquid sodium can account for crack growth in the electrolytic membrane. The balance of the dissolution fluxes determines whether the crack will grow and allows the determination of a critical current density below which crack growth should not occur. This is supported by electrolytic tests in which a critical current density below which strength degradation does not occur is identified. The factors which influence ceramic dissolution are:

1. The capillarity flux (J_γ) which arises from the higher surface solute (electrolyte) concentration at the crack faces than the crack tip. The concentration of solute in equilibrium with the crack faces will be greater than that near the tip. This will lead to dissolution of solid at the crack faces and deposition at the tip.
2. The flux arising from stress effects (J_σ). The stress changes the chemical potential of the solute (electrolyte) ions and leads to a concentration excess near the tip which tends to drive solute out of the crack.
3. The flux resulting from sodium efflux (J_E). Since sodium flows out of the crack during electrolysis it will carry the solute (electrolyte) with it.

The total flux is given by

$$J_T = J_\gamma + J_E + J_\sigma \quad (5)$$

and the capillarity flux leading to electrolyte deposition at the crack tip is opposed by the sodium efflux and stress fluxes which lead to dissolution at the crack tip. For the stress and capillarity fluxes the concentrations at the crack tip are determined from the dependence of chemical potential on each of these factors. The flux is then calculated using Fick's Law and assuming that the concentration gradient at the tip is given by the difference in concentration between the crack tip and equilibrium value divided by the crack tip radius. The mechanical stress at the crack tip is the pressure generated by the flow of sodium out of the crack tip and is determined by Poiseuille's Law.

The flux of dissolved electrolyte due to sodium efflux is calculated from the volume of sodium flowing into the crack tip and the concentration of dissolved

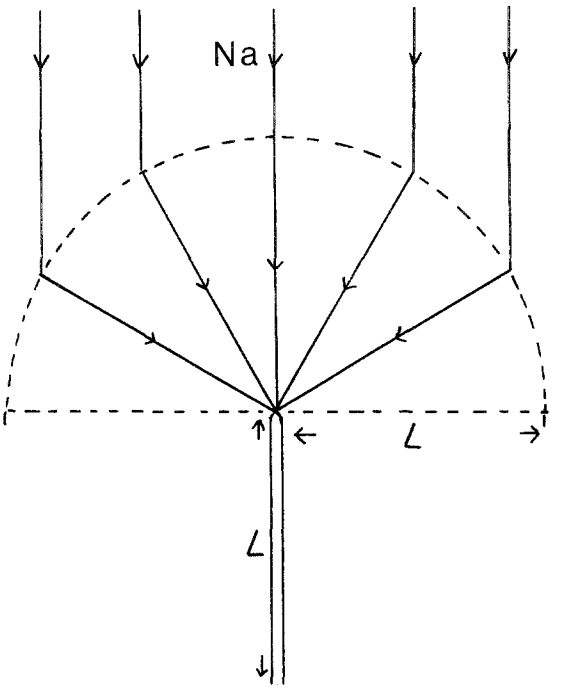

Figure 2 The Richman–Tennenhouse current focusing assumption (after Richman and Tennenhouse [2]).

electrolyte. Current focusing (Fig. 2) to the low resistance sodium crack is incorporated by assuming that any sodium ions within a distance equal to the crack depth will "see" the metal filled crack before the surface and will be directed to the crack. The flux equation consequently becomes

$$J_T = \underbrace{\left(\frac{C_0 D\Omega\gamma}{kTr^2}\right)}_{\text{Capillarity}} - \underbrace{\left(\frac{6.14 i V_m l C}{F\pi r}\right)}_{\substack{\text{Sodium}\\ \text{efflux}}} - \underbrace{\left[\frac{C_0 D\Omega l^5}{kTEr^8}\left(\frac{6.14\eta i V_m}{F}\right)^2\right]}_{\text{Stress}} \quad (6)$$

where C_0 is the equilibrium concentration of the solute in liquid sodium, C is the concentration of the solute near the interface, D is the diffusion coefficient of solute in liquid sodium, γ is the solid–liquid interfacial energy, l is crack length, r is crack tip radius, i is current density, k is Boltzman's constant, η is the viscosity of liquid sodium, V_m is the molar volume of liquid sodium, F is Faraday's constant, Ω is the atomic volume of the solid, E is Young's modulus of the solid and T is temperature.

For zero nett flux $J_T = 0$, the current i in Equation 6 is the critical value above which crack growth will occur. At $J_T = 0$, $C = C_0$ at the crack tip and C_0 can be taken out of Equation 6. The solution for the critical current density at failure i_{crit}, for a given r and l, is independent of assumptions about the solubility of the electrolyte in sodium. Two regimes can be identified based on these (r and l) dimensions. One at small crack tip radii in which the stress (J_σ) term is dominant and i_{crit} is a function of (crack length)^5. The other at larger tip radii where the sodium efflux term J_E is dominant and the critical current is a function only of (crack length)^1. Comparison of the required ceramic solubilities for the two regimes based on the

assumption of two crack tip radii (2×10^{-7} cm, J_σ dominance and 5×10^{-6} cm, J_E dependence) suggests that J_σ dominance fits the experimental data better. For J_E dominance aluminium would be detectable in the sodium and this is not found.

The rate of crack propagation is given by

$$V_{crack} = \frac{dl}{dt} = -\Omega J_T \quad (7)$$

For stress dominance this becomes

$$V_{crack} = \frac{dl}{dt} = -\Omega(J_\gamma + J_\sigma) \quad (8)$$

where V_{crack} is the crack velocity.

If crack tip radii of 2×10^{-7} cm are assumed then initial flaw lengths of 19 μm are required to give the experimentally observed value of 0.15 A cm^{-2} for 9.9% Na_2O–1.1% Li_2O, balance Al_2O_3 ceramic. For crack radii of 10^{-7} cm and crack lengths of 3.8 μm this would give the value of 1 A cm^{-2} observed experimentally for 9.25% Na_2O–0.25% Li_2O, balance Al_2O_3 ceramics. The model is essentially one of subcritical crack growth by stress assisted dissolution.

2.2.5. The Shetty–Virkar–Gordon (S–V–G) Model

Shetty *et al.* [4] gave a quantitative extension of the (A–D–T) critical crack growth mechanism using the critical fracture concept. In addition an attempt was made to remove the assumption of arbitrary crack width assumed by both the A–D–T and R–T models. They did this by considering the interdependence of the crack shape and the pressure distribution within it. This allowed the crack opening displacement to be determined by the internal pressure. In addition they introduced the critical stress intensity factor K_{Ic}, a concept which had not been explicitly used in the A–D–T model. The model is one of critical but slow fracture in which crack extension occurs when the stress intensity attains the critical value K_{Ic}.

The important feature of this approach is the iterative determination of the crack shape based on the need for consistency between the pressure distribution and crack shape. An edge crack of length l is considered and a Poiseuille pressure distribution which depends linearly on crack length is assumed. A constant sodium volume flow rate maintained in a constant width channel would give this pressure distribution. Using numerical techniques the crack face displacement was found to be constant for about half the length of the crack from the open end. The crack width then decreases to the end. The assumption of constant flow rate would lead to point focusing at the end of the channel. More realistic focusing would be over a region of the crack tip. The volume flow rate would then decrease toward the crack tip. It appears that the triangular distribution is consistent with the crack shape to a first approximation.

The crack growth kinetics during fracture were obtained by determining the Poiseuille pressure from the average exit flow rate of sodium and equating this to the pressure required by the Griffith criterion for failure of an edge crack. The average exit flow rate of sodium was found from the total inflow of sodium into the crack (determined by the R–T current focusing method) less the volume increase of the crack on fracture. The volume of the crack was determined from the crack shape numerical iteration and its time derivative, the volume increase on fracture, is related to the crack propagation rate. Consequently it was possible to relate the crack propagation rate to the current density and materials properties.

$$\frac{dl}{dt} = Al^{1/2} - Bl^{-1/2} \quad (9)$$

where

$$A = \frac{4iV_m}{3F\beta}\left[\frac{\alpha E}{(1-\nu^2)\gamma_{eff}}\right]^{1/2}$$

$$B = \frac{4\varepsilon^3(1-\nu^2)\gamma_{eff}^2}{9\beta\eta E^2\alpha^2}\left[\frac{\alpha E}{(1-\nu^2)\gamma_{eff}}\right]^{1/2}$$

where the symbols were as used earlier (Section 2.2.4) and α, β and ε were numerical constants.

The equation is only valid for $i > i_{crit}$ where i_{crit} is the value at which $dl/dt = 0$. For a polycrystalline beta-alumina the value of i_{crit} for an initial flaw size of 25 μm and a typical fracture energy of 20 J m^{-2} was given as 1500 A cm^{-2}. In a later paper Virkar and Viswanathan [20] says that there is a numerical error in the calculation and the value should be of the order of 10^4 A cm^{-2} for a flaw of length 100 μm. The value is clearly too high compared with experimentally observed critical current densities of the order of 1 to 2 A cm^{-2}. A number of possible reasons were given to explain this discrepancy:

1. The measured fracture energy might not be representative of the kind of fracture observed. The single crystal fracture energy is 1 J m^{-2} and leads to i_{crit} of 3.8 A cm^{-2}. (Significant current focusing would not, however, be observed to the same extent in the high conductivity conduction plane).
2. The effect of crack tortuosity in enhancing the Poiseuille pressure.

2.2.6. Comparison of the S–V–G and R–T models

Although large slopes are observed in the log crack velocity–log stress intensity plots for beta″-ceramics (discussed in Section 2.1.1) Shetty *et al.* [4], do not argue that the R–T model is incorrect. Mechanical stress corrosion tests in liquid sodium may not simulate the electrolysis condition. The effects of electric fields, current focusing, surface wetting conditions and the elimination of supersaturation near the surface of the electrolyte may all be important. Shetty *et al.* [4], suggest that the temperature dependence of degradation may be a test for the applicability of the two models. In the S–V–G treatment the critical current density for failure would depend on the viscosity of sodium. This dependence is given in a later paper by Virkar and Miller [21] by

$$i_{crit} = \frac{A}{\eta l} \quad (10)$$

where A is a constant containing the electrolyte elastic

and fracture properties, η is sodium viscosity and l is the length of the sodium filled crack.

In the R–T model the critical current density could either increase or decrease with current density depending on the magnitudes of the various fluxes (Equation 5). The dependence of current density on temperature was determined experimentally by Virkar and Miller [21]. They investigated the times to failure of beta″-alumina electrolytes 8.85% Na_2O–0.75% Li_2O, balance Al_2O_3 in sodium–sodium cells at temperatures between 120 and 400° C. A d.c. current was used for electrolysis and a switching system reversed the polarities after a preset time interval. The maximum current density used was 4.5 A cm^{-2}. The cells were treated at 400° C before testing to ensure proper sodium wetting. Cells operated at 300° C and 1 to 1.25 A cm^{-2} for a few hundred A h cm^{-2} did not fail and were removed from testing. Some cells were cooled to a temperature in the region 120 to 150° C and they failed at a current density of 1 to 1.25 A cm^{-2} within a few minutes. This behaviour was also seen for cells that were operated at 120° C without passing large currents at 300° C. The failure at 120° C is thus not simply an effect of total test time, but was a function of the test temperature and current density. Cracks in the ceramic were observed in the failed cells, surface craters and dimples were also observed. The ceramic darkened in some cases but the darkening did not appear to be associated with cell failure. At 400° C cells operated at current densities as high as 4.5 A cm^{-2} did not fail. The critical current density for failure at 400° C would appear to be greater than 4.5 A cm^{-2}. The critical current density at failure for cells at 120° C was not greater than 1.13 A cm^{-2}. The calculated i_{crit} for an inherent flaw of 100 μm at 300° C is 90 A cm^{-2}. The reason for this discrepancy proposed by Virkar and Miller is that the electrolyte surface is not well wetted. As a consequence of this, high local current densities caused by current intensification at the edges of non-wetted areas can exceed the applied current density by as much as 1 to 2 orders of magnitude. In the same way as the flaws on the ceramic tube may be expected to have a probability distribution resulting in a Weibull survival probability distribution so would the non-wetted areas. Virkar and Miller drew the following conclusions:

1. Sodium–sodium cells fail more readily at lower temperatures than high temperatures. Thus, it is preferable to operate cells at as high a temperature as possible consistent with other aspects of the operation and performance of the cells.
2. Non-wetted areas of the electrolyte surface can be most deleterious to cell performance. Thus every attempt should be made to improve wetting. Addition of benign impurities is one possibility.
3. A simple consideration of Weibull statistics demonstrates that cells containing smaller tubes would perform better than cells containing larger tubes. Furthermore Weibull statistics can be used to take into account preferential wetting.

2.2.7. Brennan's model

Brennan [22] considered the earlier models of electrolyte failure and introduced three refinements. The pressurized sodium develops a back e.m.f. which reduces current flow to the crack. The properties of the beta″-alumina had been assumed not to vary with time whereas in practice both the bulk and surface resistance could change. Finally an equivalent circuit treatment was used to analyse the partition of current flow between the crack and the electrolyte. In Brennan's model the electrolyte life in a cell test was not considered in terms of crack propagation rates. He suggested that as a result of various time dependent factors a state of criticality was achieved in the pre-existing flaws in the ceramic. The crack propagation after criticality was believed to be rapid. The two major factors which produced electrolyte failure were thought to be: increases in the interfacial charge transfer resistance at the sodium electrode; and high local current densities as a result of non-uniformity of electrode operation. For current densities of 10^4 A m^{-2} with the beta-alumina bulk resistance equal to 0.06 Ω m and charge transfer resistance 10^{-6} Ωm^2 the region of critical cracks was for lengths greater than 100 μm and crack tip radii less than 10 nm. Virkar *et al.* [23], in commenting on Brennan's model reiterated the need to consider the crack opening displacement as a function of pressure rather than to arbitarily fix a crack radius. On this basis they suggested that the quantitative calculations of Brennan were invalid. They argued a similarity between the charge transfer resistance increase at the surface and non-wetting. Moreover, they concluded that the back e.m.f. effect could not arise within the liquid sodium since an e.m.f. due to pressure difference can only be developed if the sodium reservoirs to which the two different pressures were applied were separated by an ionically conducting membrane. The retardation of sodium ion flux to the pressurized crack could be understood in terms of the increase in chemical potential of the pressurized sodium ion cores in the crack and the decrease in chemical potential of the sodium ions in the crack tip. Virkar *et al.* [23], also suggested that the equivalent circuit for current focusing did not represent the crack. The Brennan equivalent circuit for zero charge transfer resistance led to a tip fed crack whereas the analytical solution for this condition showed that the crack is fed from its sides.

2.2.8. Refinements of the current focusing concepts

Refinements of the current focusing calculations were carried out by Virkar [24] and by Feldman and De Jonghe [25]. Virkar solved the Laplace equation for current flow to the sodium filled crack by assuming that the sodium resistivity was zero and that the charge transfer resistance at the sodium–beta-alumina interface was also zero. The exact solution did not make a significant difference to the calculated value of the critical current density for failure. The previous value using the R–T current focusing assumption was 10^4 A cm^{-2} ([4] corrected in [20]) and the new value was 12 000 A cm^{-2}. The calculation by Feldman and De Jonghe assumed an elliptic cylindrical crack geometry which allowed straightforward

solution of the Laplace equation. The maximum current flow at the crack tip was a factor of 2 smaller than the R–T current focusing assumption. The critical current densities calculated on this basis were still much higher than the experimental values. De Jonghe and Feldman [25] rationalize the discrepancy by arguing that sodium was formed under pressure by the injection of electrons into the beta-alumina under the influence of the electric field at the crack tip. The pressurized sodium produced a lower critical stress intensity factor and this accounted for the discrepancy between the observed and experimental critical current densities for failure. In a later paper [26] it is pointed out that fracture toughness anistropy in beta″-alumina could also account for it.

Virkar's rationalization followed the approach that the actual local current densities could be significantly increased by non-wetted areas, head losses due to rough crack surfaces and the possible effect of thin channels on the sodium viscosity.

It was concluded [24] that cuirrent densities could easily be enhanced by a factor of 10 to 50. Feldman and De Jonghe [25] argued however, that although the current densities would be enhanced at the tip edge the region over which enhancement occurred would be small. The dendrite would effectively grow out of the high current density region. Their arguments were based on calculation of the current intensification around an elliptic cylindrical non-wetted region.

The problems of poor wetting of the ceramic by sodium on local current densities were investigated by Virkar, *et al.* [27]. They used an electrical mechanical analogue to determine intensification and obtained

$$i_{\text{tip}} = i\left[2\left(\frac{C}{r}\right)^{1/2} + 1\right] \qquad (11)$$

where i is current density, $2C$ is the diameter of the unwetted area and r is the crack tip radius. Bar shaped specimens of beta″-alumina 8.8% Na_2O–0.75% Li_2O, balance Al_2O_3 were treated by painting one side with silver paint and electrolysing sodium to this cathode at a current density of 50 mA for 1 min from a solution of sodium nitrate in water at room temperature. The strength of the bars was determined by breaking in bending and found to be 170 MNm^{-2} for non-electrolysed samples and 132 MNm^{-2} for electrolysed samples. A small non-wetted area was simulated by a non-silver painted area of radius 0.15 cm in the centre of the bar. The strength of the bar after test was 55 MNm^{-2} indicating that considerable current intensification had occurred. (The reduction in electrode area was only 1.5%). Current focusing was demonstrated practically by machining a crack in the beta-alumina, coating with silver and electrolysing sodium to the cathode from sodium nitrate in water at room temperature. Sodium streaks formed from the tip of the crack verifying the current focusing in the A–D–T, R–T and S–V–G models.

2.2.9. The three-dimensional crack model (Virkar and Viswanathan [20])

Virkar and Viswanathan's [20] most recent contribution to the critical fracture model was to consider the

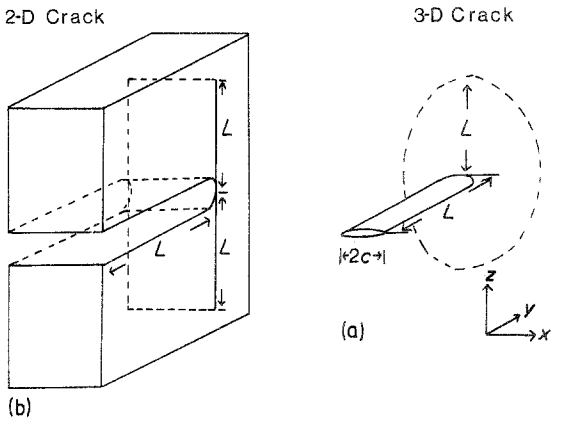

Figure 3 (a) Three-dimensional crack model. (b) The two-dimensional model is shown for comparison (after Virkar and Viswanathan [25]).

situation which would exist for a three-dimensional crack. Such a crack is illustrated in Fig. 3 where it is compared with the cracks of a two-dimensional type which have already been discussed. The consideration of a three-dimensional crack in a cube of material under uniform tension in the z direction and the application of St Venant's principle shows that such a crack will extend in the x direction rather than along the length of the crack (the y direction, Fig. 3). The critical dimension which determines the crack extension is consequently the crack width not its length. Earlier calculation had shown [24] that the exact solution of the Laplace equation did not significantly alter the critical current density as compared with the simple R–T ion focusing concept. This allowed the assumption that ions lying in a circular region, centred on the crack tip in a plane perpendicular to the electrode surface, would be focused to the crack. The effect of this current focusing to a three-dimensional crack is very significant in that it leads to a considerable reduction in the critical current density. Applying similar arguments to those used for the two-dimensional case Virkar and Viswanathan [20] showed that the maximum pressure which occurs at the crack tip is given by

$$P_0 = \left[\frac{2\eta V_m E^3 l^3}{(1-\nu^2)^3 F c^4}\right]^{1/4} (i)^{1/4} \qquad (12)$$

where P_0 is the maximum pressure at the crack tip, η is sodium viscosity, V_m is the molar volume of sodium, E is Young's modulus for beta-alumina, l is the crack length, ν is Poisson's ratio, F is Faraday's constant, $2c$ is the crack width and i is the average applied current density.

The crack tip pressure is proportional to $l^{3/4}$. The crack extension would be expected in the x direction (width of the crack) rather than in the y direction (length of the crack) if the loading were uniform. The loading, however is not uniform and so the crack was expected to extend in the y direction (along its length). Equating the maximum pressure to the pressure required for fracture on the basis of the Griffith equation for a penny-shaped crack (i.e. considering the crack tip region) gave

$$i_{crit} = \left[\frac{\pi(1-\nu^2)F\gamma_{eff}^2}{8V_m E\eta}\right]\left(\frac{c^2}{l^3}\right) \quad (13)$$

where γ_{eff} is the surface energy.

The crack width ($2c$) is incorporated more simply into the equation than in the two-dimensional calculations and i_{crit} is a function of l^{-3} rather than l^{-1} in the two-dimensional case. The equation simplifies on substitution of the constants with $\gamma_{eff} = 5\,J\,m^{-2}$ to

$$i_{crit} = 16.73 \times 10^4 \left(\frac{c^2}{l^3}\right) \quad A\,cm^{-2}$$

For a crack length of 100 μm and width of 60 μm, i_{crit} was 151 A cm^{-2}. For a 200 μm length crack with width 60 μm, i_{crit} was 18.8 A cm^{-2}. It must be appreciated that although the authors included an arbitrary flaw width, the crack opening displacement is automatically built into the analysis. The two factors of major significance in the three-dimensional mode are: (a) the failure stress does not depend on crack length but on the minor dimension, crack width and (b) the effect of ion focusing is greater in comparison with the two-dimensional model if $l \gg 2c$.

The order of magnitude calculation presented demonstrated that values of i_{crit} similar to experimental values could be obtained by the three-dimensional model. Experimental results in the paper gave values between 10 and 20 A cm^{-2}.

2.2.10. The effect of microstructure on Mode I failure

Virkar and Viswanathan [20] considered the effect of microstructure on the Mode I degradation in the same paper as their three-dimensional model. They considered the effect of the grains in increasing the tortuosity of the surface crack. There were two effects, one the head loss at bends, the other the increase in effective crack length. The former effect was found to have little effect on the critical current density. The latter affected the critical current density through the cosine of the angle (θ) at which the crack deviated from its normal path; for $\theta = 45°$ the critical current density for a crack 200 μm long with width 60 μm was 12 A cm^{-2} rather than 19 A cm^{-2} for a straight crack. Buechele *et al.* [28] carried out an investigation of the effect of microstructure on Mode I failure using an acoustic emission technique similar to that first used for studying electrolytic degradation by Worrell and Redfern [29]. Sodium–sodium cells with ceramic coated with insulating glass except in a 0.2 cm^2 area were used. The ceramic composition was 8.8% Na_2O–0.75% Li_2O, balance Al_2O_3. A fine grained ceramic and a coarse grained ceramic were used. Although both microstructures were bimodal the volume fraction of grains greater than 10 μm was less than 0.01 in the fine grained material as opposed to 0.83 for the coarse grained material.

The cells were operated at 350° C and the current density increased until failure occurred. Two criteria were used for failure, the first significant acoustic emission above background and the start of sustained acoustic activity. It was believed that the onset of sustained acoustic activity involved flaw extension. A particularly significant feature of the work of Buechele *et al.* was the use of Weibull statistics to interpret the failure data. The flaws in the ceramic surface would be expected to be statistically distributed. The largest flaw would be expected to grow first under the influence of the applied current density and so the appropriate distribution would be the Weibull. The distribution of flaw sizes would lead to a distribution of current densities at failure. Consequently the survival probability would be related to the critical current density by

$$P_s = \exp\left[-\int_A \left(\frac{i-i_u}{i_0}\right)^n dA\right] \quad (14)$$

where P_s is the survival probability, A is the sample surface area, i is current density, i_u is current density below which failure does not occur, i_0 is a normalizing constant and n is the Weibull coefficient.

It was assumed that $P_s = 1$ when $i_u = 0$. The authors pointed out that this is not valid but i_u cannot readily be calculated from their data although an upper bound of 20 mA cm^{-2} can be estimated.

Using the various current densities for failure on the acoustic emission criterion for samples from each microstructural type it was possible to construct Weibull plots of survival probability against current density at failure. The average critical current density for failure ($P_s = 0.5$) was found to be 145 mA cm^{-2} for large grained samples and 640 mA cm^{-2} for small grained samples. Extension of the electrical mechanical analogy led the authors to suggest that proof testing would be necessary to ensure that ceramics did not fail in service. They pointed out that this suggestion was made on the assumption of the equivalence of electrical and mechanical failure which they believe does not hold completely. In addition the criteria of electrolyte failure in the laboratory are different from those used by the battery developer.

2.2.11. Mixed Mode I and Mode II degradation – a supersaturation model (*Kuribayashi and Nicholson* [30])

Kuribayashi and Nicholson [30] have proposed a supersaturation model for the electrolytic degradation of beta-alumina. As a result of current focusing to the sodium filled cracks of the beta-alumina and because only some grains will have their conduction planes correctly oriented for sodium ion discharge, the available conduction planes become saturated with Na^+ ions. Since the ions cannot be discharged quickly enough they react within the conduction plane. The sodium ions react with the conduction plane oxygen ions to give sodium and oxygen.

$$Na_{Na} + O\,(5) \rightarrow Na + (O_0)^{\cdot} + V'_{Na} \rightarrow Na + \\ + O + (e)'_0 + V'_{Na} \quad (15)$$

(where O(5) is the conduction plane oxygen ion and Kroger-Vink notation has been used).

The oxygen released may dissolve in the liquid sodium or form sodium oxide. The colloidal sodium or sodium oxide formed within the structure will lead to microcracking allowing further colloid growth. If

the colloids extend back to the original sodium filled crack a dendrite is produced.

Nicholson [31] demonstrated the feasibility of the supersaturation model by considering current focusing to a two-dimensional 20 μm flaw. This allowed the calculation of the number of sodium ions arriving per sec. On the basis of a 20 μm grain size, consideration of the volume influenced by the flaw and estimates of the number of correctly oriented grains, he calculated the number and total area of conduction planes feeding the flaw. From structural considerations and the known site occupancy a figure for the available sites was calculated. The number of sodium atoms arrived exceeded the number of available sites and so the possibility of saturation existed.

By taking the number of conduction planes per flaw, the assumed dimensions of the grain and the intersite distance, he calculated the number of sites at the sodium exit line into the flaw. This number was then compared with the number of sodium atoms arriving within the residence time for each site at the various current densities.

Saturation was approached at 2.5 A cm^{-2} for beta-alumina. Beta″-alumina was not saturated at 2.5 A cm^{-2}. Factors which could increase the likelihood of supersaturation were (a) channelling of excess sodium ions from beta- to beta″-, (b) impurities blocking the conduction plane by the mixed ion effect and (c) decrease in the number of available sites due to non-stoichiometry. Nicholson and Kuribayashi [30, 32] supported their model by a number of experiments. They subjected bar-shaped, notched samples to tensile and compressive stress. The electrode system consisted of silver paint as the negative electrode and a $NaNO_2/NaNO_3$ eutectic as the positive electrode. They used MgO stabilized beta″-alumina samples of composition 11.1% Na_2O–1.93% MgO, balance Al_2O_3. A drop in K_{Ic}, the critical stress intensity factor was observed when samples were electrolysed for 30 min at 2 A cm^{-2}. At lower current densities both tensile and compressive stresses reduced the K_{Ic} value at which fracture occurred.

At a fixed current density of 0.3 A cm^{-2} with 150 MPa tensile stress at the notch tip degradation was enhanced at higher temperatures. At constant stress the time to failure t_f was related to temperature, log $1/t_f$ varied linearly with $(1/T)$ which gave an apparent activation energy of 28 k J mol^{-1}. The value is close to the value 21 k J mol^{-1} for sodium ion diffusion which suggested that sodium ion diffusion controlled the degradation rate.

Nicholson [31] argued that the Poiseuille pressure models were incorrect since:

1. the temperature dependence of deterioration was incorrect;
2. low K_I values were obtained for normal current densities;
3. K_{Ic} was reduced under compressive stress (K_{Ic} would be expected to increase under compression on the Poiseuille pressure models);
4. the current densities predicted by the Poiseuille pressure models for failure were unreasonably high.

3. The anodic decomposition of beta-alumina

Although much work has been carried out on the reactions occuring during the deposition of sodium at the cathode the anodic decomposition reactions have not been neglected. One of the most detailed studies was carried out by Armstrong *et al.* [33]. They considered reactions

$$Na_2O \cdot 11\,Al_2O_3 \rightarrow 2Na + \tfrac{1}{2}O_2 + 11\,Al_2O_3 \qquad (16)$$

which are thermodynamically feasible above 2.0V but which were believed to be limited by the anodic reaction (the liberation of oxygen ions from the beta-alumina lattice).

3.1. Anodic decomposition at high potentials

The effects of anodic decomposition at high potentials are of relevance to operation of strings of cells in batteries. Hooper [34] investigated sintered ceramic discs over a temperature range of 100 to 375° C which had been subjected to voltages between 56 and 125V. The potential of the sample was increased in 2 V steps until "breakdown" (a sudden increase in sample current) was observed. The conclusions for blocking electrode materials (ones which do not allow ion transport) were that the breakdown voltage was; (a) independent of sample thickness, (b) independent of electrode material, (c) independent of surface roughness and (d) reproducible.

Lower breakdown voltages were observed at higher temperatures (56V at 375° C, 125V at 100° C). Fine grained ceramic exhibited less temperature dependence of the breakdown voltage than the coarse grained ceramic. Visual and microscopic investigation revealed that gross damage had occurred at the positive electrode surface. It was proposed that the damage was caused by the dielectric breakdown of a thin sodium ion depletion layer under the d.c. bias conditions. Tang and Chaudhri [35] found breakdown at values above a critical voltage of 800 V for single crystals of beta-alumina and 270 V for polycrystalline beta-alumina. They identified three modes of degradation:

1. sodium formation caused by electron injection to beta-alumina from the cathode as a result of high local fields due to cathode polarization, as polarization proceeds;
2. the anode field increases and sparks occur at the anode, resulting in the formation of sodium and possibly oxygen;
3. the transient increase in current density during a spark leads to filamentary sodium growth at the cathode.

3.2. Anodic decomposition at low potentials

Armstrong *et al.* [33] investigated the complex plane impedence spectrum of beta-alumina at 25° C in the cells carbon/beta-alumina/NaI/I_2(Pt) and Au/beta-alumina/NaI/I_2(Pt) as a function of anode potential up to 8 V with respect of NaI/I_2(Pt). They showed that the impedance spectrum was essentially unchanged up to 8V.

The equivalent circuit [33] for the cell which had sodium ion reversible reference and counter electrodes was a parallel combination of the bulk resistance and geometric capacity, in series with the double layer capacity (C_{dl}). At low frequencies this reduced to C_{dl} in series with the bulk specimen resistance and the observed impedance spectrum corresponded to this equivalent circuit. The value of C_{dl} was 3×10^{-7} F cm^{-2}. The invariance of the capacitance with potential indicated that the anodic reaction in Equation 16, which was to be expected on a thermodynamic basis, did not occur because it was substantially limited by the kinetics of transfer of an oxygen ion from the beta-alumina lattice. Mitoff and Charles [36] worked at 596° C and found that the measured capacitance was about 10^{-3} F cm^{-2}. They believed that the experimental data could be explained by the inclusion of absorption and diffusion terms. Aceves *et al.* [37] worked at 400° C with the Au/beta-alumina/Au cell with potentials of up to 12V and found that their capacitances were six orders of magnitude greater than Armstrong's. They speculated that sodium is discharged at the cathode and that oxidation of the beta-alumina takes place at the anode. It appeared that oxygen gas was not liberated at the anode. It seemed that the beta-alumina framework was partially oxidized but retained its integrity. This could occur if only one electron of the oxygen ion was removed and it remained attached to an aluminium ion. The authors suggested that such an anodic reaction may occur on charging of the sodium–sulphur cell and observed that their samples sometimes powdered after several polarization cycles in the Au/beta-alumina/Au cell.

Zeising *et al.* [38] carried out cyclic voltammetry with a sodium amalgam reference electrode to determine the reactions at the sodium amalgam/beta-alumina interface and the platinum/beta-alumina interface at 210° C. The behaviour of the platinum/beta-alumina interface on anodic polarization at 210° C was not in agreement with the observations of Armstrong *et al.* [33] on gold and carbon interfaces at 25° C. Zeising *et al.* [38] found that an oxidation reaction (Equation 17) started at 3.5V with respect to the sodium amalgam reference electrode giving a decomposition potential of 3.0V.

$$Na_2O \text{ (in beta-alumina)} \rightarrow 2Na\text{–}Hg + \tfrac{1}{2}O_2 \qquad (17)$$

This was in agreement with a value found earlier by Tannenberger [39].

Bovin and O'Keefe [40] have investigated the loss of sodium from the ceramic near the anode which accompanies anodic breakdown using a high resolution transmission electron microscope (HRTEM). Loss of sodium from the interior of a crystal results in conversion of the conduction planes into non-conducting regions of aluminium oxide. This was observed by Bovin both as a result of electron beam damage and in the cycled electrolyte. Gupta and Tennenhouse [41] highlighted the damage which occurred as a result of non-uniform sulphur electrode operation. They found that when sulphur electrodes with different graphite felt shapes were used the fracture pattern of the ceramic related to the electrode shape. Whilst they attributed failure to the local high current densities arising from electrode non-uniformity it is possible that some effect of anodic decomposition is present. De Jonghe *et al.* [18] mention an imprinting effect on the sulphur electrode side of the ceramic where the light and dark regions on the electrolyte surface reflect the shape of the graphite felt of the sulphur electrode. Using the silver decoration technique the authors showed that a band of degradation was present at the sulphur electrode surface. The uniformity of the layer increased with cycling. De Jonghe *et al.* did not advance an explanation of the sulphur side layer.

4. The chemical effects of sulphur and polysulphides

The degradative effects of sulphur and polysulphides on the beta-aluminas do not appear to be very significant. Early work established compositions in which sulphur and polysulphide attack was negligible [42]. Recently Smaga and Battles [43] have investigated the effects of a range of polysulphides on the chemical stability of polycrystalline beta-aluminas. The polycrystalline samples were of two compositions 8% Na_2O–2% MgO and 90% Al_2O_3 (0.6β, 0.4β''), and 8.85% Na_2O–0.75% Li_2O and 90.4% Al_2O_3 (β''). On correction of the data for weight increases associated with potassium uptake no net weight change was observed on exposure to polysulphide for 167 days at 350° C. The samples were not discoloured and their surface appearance even at high magnification was unchanged. Smaga and Battles [43] concluded that any sulphur electrode degradation of beta-alumina must be electrochemical in origin. (By employing weight change measurements and scanning electron microscopy of the sample surface Smaga and Battles found evidence for beta-alumina dissolution in sodium at 350° C. For Li_2O stabilized beta-alumina, 0.6 wt % dissolved in sodium and 1.2 wt % in sodium oxide saturated sodium. For MgO stabilized beta-alumina, 0.9 wt % dissolved in sodium and 1.2 wt % in sodium oxide saturated sodium. The surface degradation was rapid and levelled off once a solubility limit in the sodium was attained. This tends to support earlier arguments (Sections 2.1.2 and 2.2.4).

5. The role of impurities in the degradation of beta-alumina

The harmful effects of impurities on ceramic performance and reliability have long been recognized. Lazennec *et al.* [44] found that potassium impurities exchanged with sodium ions of the beta-alumina lattice. The potassium has a marked influence on both the ageing and lifetime of the ceramic. The potassium produces an expansion in the *c* parameter of the beta-alumina lattice and the cells fail catastrophically. The breakdown did not appear to depend on electrolysis, the lifetime before breakdown was the same in cycled and uncycled cells. Observed increases in resistance were attributed to ion blocking effects associated with the incorporation of potassium ions into the beta-alumina lattice. Yasui and Doremus [45] investigated

the distribution of potassium ions introduced by ion exchange into beta-alumina. They found non-uniform uptake of potassium with large grains containing the equilibrium amount of potassium surrounded by small grains which did not contain any.

In a further study Yasui and Doremus [46] found that of three impurities studied iron showed no effect potassium (0.2%) increased cell impedance by a factor of 2 to 3 but that calcium was an extremely damaging impurity. The impurities were added as the sulphides in the sulphur compartment. Small amounts of calcium in the melt (0.05%) led to large increases in the cell impedance and concentration of calcium in the grain boundaries. This appeared to cause the cracking of the ceramic. The significant role of low levels of impurities was further emphasized by a study of the phenomenon of resistance rise.

5.1. Resistance rise

This form of ceramic degradation shows itself as an increase in cell resistance with time [47] and the appearance of assymetry [47, 48], that is a higher discharge resistance than charge resistance. Park *et al.* [49] have given a detailed analysis of the kinetics of resistance ageing and find it splits into three parts, an initial stage I where the resistance falls due to wetting, stage II a slow resistance rise due to bulk impurity (e.g. water) diffusion and stage III a rapid resistance rise due to surface degradation or sulphur electrode effects.

Demott [48] showed that replacement of the sodium and cleaning of the beta-alumina surface which had been in contact with the sodium electrode by scraping and washing with ethanol, was effective in reducing the resistance of cells which exhibited resistance rise. Breiter *et al.* [47] showed, by using a cell Na/beta-alumina/$NaNO_3$ containing a sodium reference probe in a hole drilled in the beta-alumina ceramic, that the increase in discharge resistance was associated with the sodium–beta-alumina interface. They attributed the resistance rise to the formation of a thin passivating film of Na_2O at the interface. In a later paper Demott *et al.* [50] suggested that material was eluted out of the ceramic "poisoning" the beta-alumina surface. In the absence of improved ceramic, a surface treatment method in combination with an oxygen getter in the sodium electrode was used to maintain resistance stability. The surface treatment of the ceramic with lead acetate improved wetting and resistance stability when used in combination with an oxygen getter such as titanium or aluminium sponge. This enabled low and stable cell resistances to be obtained.

Investigation [51] of the surface of beta-alumina tubes from sodium–sodium cells showing resistance rise, using electron microprobe measurements, demonstrated a surface enrichment of calcium by up to 100 times above the level of impurity in the bulk (a few hundred p.p.m.). X-ray photoelectron spectroscopic (XPS) and Auger measurements showed that a 400 nm thick surface layer of calcium containing material was present. They concluded that the assymetry did not require the passage of current for its development only contact with sodium was needed. Keddar *et al.* [52] suggested on the basis of XPS measurements that the surface layer contained CaO and $Ca_3Al_2O_3$.

The harmful effects of calcium either in the sulphur electrode or the ceramic were established. Breiter *et al.* [53] investigated the effect of calcium within the sodium electrode and found that a cell containing 200 p.p.m. of calcium in the sodium showed significant resistance rise. The cells they used were electrolytically filled with sodium from a nitrate melt, the sodium electrode compartment being inside the tube and containing the added calcium impurity. Pitting was observed on the outside of the tube after electrolytic filling to such an extent that only tubes with final calcium concentrations less than 200 p.p.m. could be made into sodium–sulphur cells. It was thought that the internal formation of a calcium rich resistive layer caused focusing through deposit free areas. Locally high current densities and consequent Joule heating were believed responsible for the pits.

5.2. The effect of moisture

The beta-aluminas are sensitive to moisture. Will [54] found using a.c. conductivity techniques that there was a rapid exothermic occlusion of water by surface micropores which causes saturation in less than 1 h. This was followed by slow diffusion of H_3O^+ ions into the lattice leading to ion exchange with sodium. The latter process is not saturated within days. Flor *et al.* [55] using thermogravimetric and X-ray techniques substantiated this but concluded that the rapid penetration takes place in the first few microns near the conduction plane boundaries. In addition they found that the water desorbed between 100 and 250° C. The effect of water absorption was to cause a c lattice parameter change in the beta-alumina. Heavens [56] investigated the X-ray diffraction of polycrystalline beta-alumina. He found surface layers up to 5 μm deep with a lattice distortion of the c axis of about 1%. The surface layer was produced by the replacement of Na^+ ions by H_3O^+ ions on exposure of the beta-alumina to air. Dunn [57] showed that exposure of ceramic tubes to flowing air caused resistances to increase considerably and to become non-ohmic after 2 days. He postulated a hydrated layer and found it was removed by heating to 600° C in dry air. Evolution of carbon dioxide was observed at higher temperatures which implied further chemical reaction. Armstrong and Sellick [58] found that the a.c. impedance of polycrystalline samples was moisture sensitive. Hunter *et al.* [59] investigated the surface layers on polycrystalline beta-alumina and proposed that a pre-existing dealkylized layer was present on the beta-alumina and that the hydration of this layer accounts for the observed specimen impedance spectrum.

The sensitivity of beta-aluminas to moisture must be taken into account when carrying out experiments with this material.

6. Conclusions

The effect of sodium on the degradation of beta-alumina ceramic has received considerable attention in the literature and two main types of degradation

have been found: (a) failure associated with sodium dendrites and (b) failure associated with the development of electronic conductivity and the internal deposition of sodium.

Credible theories to account for the degradation have been advanced for both cases.

The effect of sulphur and polysulphides has not been investigated to the same extent and it is believed that the beta-aluminas are relatively stable to chemical attack in these melts. There are definite effects of anodic degradation at high voltages and there is some evidence for this at low voltages (at cell operating temperatures). The detailed kinetic limitations of anodic degradation are not fully understood nor are the electrochemical aspects of sulphur electrode degradation of the ceramic.

Foreign ion impurities can lead to ceramic cracking and resistance instability. The absorption of water can significantly affect ceramic resistance and life (probably as a result of subsequent poor wetting of the ceramic by sodium).

Finally it should be stressed that the reliability of the ceramic is, and would be expected to be, dependent on the inherent flaw population within the ceramic.

The improvements in understanding of the degradative processes have shaped the development of sodium–sulphur cells. Commerical cell technology is such that cells can now be made with low, stable and reproducible resistances and high reliability.

Acknowledgements

The author acknowledges helpful discussions with his former colleagues at Chloride Silent Power Ltd. Mr R. J. Bezzant of Glasgow College of Technology for the provision of departmental facilities, Mrs M. Quinn and Mr W. Russell of Glasgow College of Technology Library for help and assistance and Dr P. A. Bather for reading the manuscript.

References

1. R. STEVENS and J. G. P. BINNER, *J. Mater. Sci.* **19** (1984) 695.
2. R. H. RICHMAN and G. J. TENNENHOUSE, *J. Amer. Ceram. Soc.* **58** (1975) 63.
3. R. D. ARMSTRONG, T. DICKINSON and J. TURNER, *Electrochimica Acta* **19** (1974) 187.
4. D. H. SHETTY, A. V. VIRKAR and R. S. GORDON, in Proceedings of an International Symposium on Fracture Mechanics of Ceramics entitled "Fracture Mechanics of Ceramics" Vol. 4 edited by R. C. Bradt (Plenum Press, New York, 1978) p. 651.
5. R. W. DAVIDGE, G. TAPPIN, J. R. McLAREN and G. J. MAY, *Amer. Ceram. Soc. Bull.* **58** (1979) 771.
6. A. GIBSON, in "Power Sources 6" edited by D. H. Collins (Academic Press, London, 1977) p. 673.
7. L. VISWANATHAN and A. V. VIRKAR, *J. Mater. Sci.* **17** (1982) 753.
8. D. S. DEMOTT and B. A. W. REDFERN, *J. Physique (c)* **37** (1976) 423.
9. J. R. RASMUSSEN, G. R. MILLER and R. S. GORDON, Spring Meeting of the Electrochemical Society, Montreal, 1982. Extended abstracts 82–1, Abstract No. 720 (The Electrochemical Society, Pennington, New Jersey, 1982) p. 1153.
10. L. C. De JONGHE and A. BUECHELE, *J. Mater. Sci.* **17** (1982) 885.
11. L. C. De JONGHE, *J. Electrochem. Soc.* **129** (1982) 752.
12. L. C. De JONGHE and L. FELDMAN, *Mater. Res. Bull.* **15** (1980) 777.
13. N. WEBER, *Energy Conversion* **14** (1974) 1.
14. D. GOURIER, A. WICKER and D. VIVIEN, *Mater. Res. Bull.* **17** (1982) 363.
15. J. P. BARRETT, D. GOURIER and D. VIVIEN, *Solid State Ionics* **13** (1984) 267.
16. L. C. De JONGHE, A. BUECHELE and M. ARMAND, *ibid.* **9/10** (1983) 165.
17. A. E. McHALE, J. A. KILNER and B. C. H. STEELE, Proceedings of the 3rd International Conference on Transport in Non-Stoichiometric Compounds, State College, Pensylvannia State University, June 1984, edited by G. Simkovich (Plenum Press, New York) to be published.
18. L. C. De JONGHE, L. FELDMAN and A. BUECHELE, *J. Mater. Sci.* **16** (1981) 780.
19. L. C. De JONGHE, *Solid State Ionics* **7** (1982) 61.
20. A. V. VIRKAR and L. VISWANATHAN, *J. Mater. Sci.* **18** (1983) 1202.
21. A. V. VIRKAR and G. R. MILLER, in "Fast Ion Transport in Solids", edited by P. Vashita, J. N. Mundy and G. K. Shenoy (Elsevier–North Holland, New York, 1979) p. 87.
22. M. P. J. BRENNAN, *Electrochimica Acta* **25** (1980) 621.
23. A. V. VIRKAR, G. R. MILLER and R. S. GORDON, *ibid.* **26** (1981) 1023.
24. A. V. VIRKAR, *J. Mater. Sci.* **16** (1981) 1142.
25. L. A. FELDMAN and L. C. De JONGHE, *ibid.* **17** (1982) 517.
26. L. C. De JONGHE and D. C. HITCHCOCK, *J. Amer. Ceram. Soc.* **66** (1983) C 204.
27. A. V. VIRKAR, L. VISWANATHAN and D. R. BISWAS, *J. Mater. Sci.* **15** (1980) 302.
28. A. C. BUECHELE, L. C. De JONGHE and D. HITCHCOCK, *J. Electrochem. Soc.* **130** (1983) 1042.
29. C. A. WORRELL and B. A. W. REDFERN, *J. Mater. Sci.* **13** (1978) 1515.
30. K. KURIBAYASHI and P. S. NICHOLSON, *ibid.* **18** (1983) 1590.
31. P. S. NICHOLSON, *ibid.* **18** (1983) 1597.
32. *Idem, Can. Metall. Quart.* **23** (1984) 65.
33. R. D. ARMSTRONG, R. A. BURNHAM and P. M. WILLIS, *J. Electroanal. Chem. Interfacial Electrochem.* **79** (1980) 134.
34. A. HOOPER, *Trans. J. Brit. Ceram. Soc.* **79** (1980) 134.
35. T. B. TANG and M. M. CHAUDHRI, *J. Mater. Sci.* **17** (1982) 157.
36. S. P. MITOFF and R. J. CHARLES, *J. Appl. Phys.* **43** (1972) 927.
37. J. M. ACEVES, B. G. COOKSLEY and A. R. WEST, *J. Electroanal. Chem.* **90** (1978) 295.
38. J. ZEISING, C. VANVOREN and J. L. SOUQUET, *Electrochimica Acta* **26** (1981) 145.
39. H. TANNENBERGER, in "Fast Ion Transport in Solids", quoted by R. Galli, edited by W. Van Gool (North Holland, Amsterdam, 1973) p. 552.
40. J. O. BOVIN and M. O'KEEFFE, *Naturwissenschaffen* **66** (1979) 576.
41. N. K. GUPTA and G. J. TENNENHOUSE, *J. Electrochem. Soc.* **126** (1979) 1451.
42. G. J. TENNENHOUSE, R. C. KU, R. H. RICHMAN and T. J. WHALEN, *Bull. Amer. Ceram. Soc.* **54** (1975) 523.
43. J. A. SMAGA and J. E. BATTLES, *J. Mater. Sci. Lett.* **4** (1985) 553.
44. Y. LAZENNEC, C. LASNE, P. MARGOTIN and J. FALLY, *J. Electrochem. Soc.* **122** (1975) 734.
45. I. YASUI and R. H. DOREMUS, *J. Amer. Ceram. Soc.* **60** (1977) 296.
46. *Idem, J. Electrochem. Soc.* **125** (1978) 1007.
47. M. W. BREITER, B. DUNN and R. W. POWERS, *Electrochemica Acta* **25** (1980) 613.
48. D. S. DEMOTT, *J. Electrochem. Soc.* **127** (1980) 2312.
49. D. S. PARK, R. W. POWERS and M. W. BREITER, *Solid State Ionics* **5** (1981) 271.

50. D. S. DEMOTT, M. L. WRIGHT and M. D. HAMES, "Extended Abstracts of the Electrochemical Society", Minneapolis, Meeting May, 1981, Abstract No. 469 (The Electrochemical Society, Pennington, New Jersey, 1981) p. 1161.
51. G. LEHNERT and B. HARTMANN, "Extended Abstracts of the Electrochemical Society", Vol. 82–2, Detroit Meeting, October, 1982, Abstract No. 335 (The Electrochemical Society, Pennington, New Jersey, 1982) p. 539.
52. N. KEDDAR, D. L. KIRK and S. C. JOHNSON, *Phys. Status. Solidi* **82** (1984) 327.
53. M. W. BREITER, N. S. CHOUDHURY and E. L. HALL, *Solid State Ionics* **14** (1984) 225.
54. F. G. WILL, *J. Electrochem. Soc.* **123** (1976) 834.
55. G. FLOR, A. MARINI, V. MASSAROTTI and M. VILLA, *Solid State Ionics* **2** (1981) 195.
56. S. N. HEAVENS, *J. Mater. Sci.* **17** (1982) 965.
57. B. DUNN, *J. Amer. Ceram. Soc.* **64** (1981) 125.
58. R. D. ARMSTRONG and D. P. SELLICK, *J. Appl. Electrochem.* **9** (1979) 623.
59. C. C. HUNTER, M. D. INGRAM and A. R. WEST, *J. Mater. Sci. Lett.* **1** (1982) 522.

Received 24 June
and accepted 10 July 1985